technologically important class of problems that involve strong discontinuities and/or much weaker velocity gradients. During deformation, a material's stress conditions may undergo competition between thermal softening and combined rate and work hardening. For such a material, the eventual plastic strain for final stress collapse[2], ε_{cr}^{p}, due to thermal instability is

$$\varepsilon_{cr}^{p} = \varepsilon_{\max}^{p} + \sqrt{\left(\frac{2m\sigma^{e}}{-\pi\sigma^{e}_{\varepsilon^{p}\varepsilon^{p}}} \right)_{\max}} \ln\left(\frac{1}{\beta}\right) \qquad (1)$$

where $\varepsilon_{\max}^{e}$ is the plastic strain corresponding to the peak in the adiabatic stress-strain curve, m is the so-called strain-rate sensitivity and β is given as a non-dimensional measure of the local variation in plastic strain rate gradient. In Eq. (1), derivatives with respect to plastic strain are denoted by a subscript ε^{p}, while the subscript *max* denotes quantities evaluated at the peak (or maximum) stress conditions.

Within the context of a finite element analysis, generalization of the non-dimensional velocity perturbation, β, seems to be most straight forward when interpreted as a variation in effective strain rate within the neighborhood of any particular element (with respect to a typical finite-element discretization). When the maximum stress is reached in any particular finite (i^{th}) element, β is calculated as

$$\beta^{i} = \frac{\dot{\varepsilon}^{i} - \dot{\varepsilon}^{avg}}{\dot{\varepsilon}^{avg}} \geq 0 \text{ where } \dot{\varepsilon}^{avg} = \frac{1}{\alpha}\sum_{j=1}^{\alpha} \dot{\varepsilon}^{j}, \qquad (2)$$

and α is determined by the local connectivity of elements so as to include all neighboring elements. Here we have considered not just local strain rate, but the simple average of strain rates in the surrounding region as the background against which we measure fluctuations.

2. Experiments

Any specimen with a well-characterized geometric defect, i.e., perturbation, can exhibit stress collapse due to adiabatic shear banding, provided the material itself is susceptible to shear localization. In the context of the present investigation, a geometry that has been utilized previously in laboratory dynamic compression tests is the "tilted" cylinder[3], shown in cross-sectional view in Figure 1. The specimens are cylindrical compression specimens cut at a slight angle α. The tilt creates a non-uniform load across the top and bottom surfaces of the specimen as it is compressed, leading to a zone of concentrated shear. Deformation in the shear zone can be localize and lead to failure, which can be reflected in the measured load-displacement curve. A larger tilt corresponds to a larger perturbation and results in earlier stress collapse and failure.

For the present study, a variation of the tilted cylindrical specimen, i.e., tilted *cuboidal* (4-sided) specimens, were subjected to dynamic compression in a split Hopkinson bar apparatus. This geometry was chosen because deformation can be adequately modeled with a plane stress (two-dimensional) approximation even with the introduction of tilt. It may be noted that the introduction of tilt in the standard (cylindrical) specimen renders the problem fully three-dimensional.

The present tests were performed with tilt angles α = 0°, 3° and 6°. The specimens were electro-discharge machined from a military grade Ti-6Al-4V alloy plate and were 10 mm in both height and width. Specimen contact surfaces were lubricated with a Molybdenum grease to minimize friction, which can lead to barreling and inhibit the formation of the shear band in the desired manner.

3. Finite Element Analyses

Fully-coupled thermomechanical plane stress finite element analysis (FEA) of the titanium alloy Ti-6Al-4V tilted cuboidal specimens with α = 0°, 1°, 3° and 6° was performed with the ABAQUS/Explicit finite element code. Consistent with the experimental conditions, the height and width of the specimens analyzed was each equal to 10 mm. Figure 2a shows one of the finite element models considered (α = 3°) for illustrative purposes.

Nodes along the bottom edge were constrained from moving in the vertical (2-) direction and a velocity boundary condition was applied to the top surface. It may be noted that the elements sensitive to localization and ultimate failure are approximately square; elements with higher aspect ratio are far removed from the localization-critical regions.

The rate-dependent Johnson-Cook plasticity model, given by

$$\sigma = \left[A + B\varepsilon^{n}\right]\left[1 + C\ln\left(\frac{\dot{\varepsilon}}{\dot{\varepsilon}_{0}}\right)\right]\left[1 - \left(\theta^{*}\right)^{m}\right] \qquad (3)$$

was used to model the titanium alloy used for the experiments, with A = 1.05 GPa, B = 1.9 GPa, n = 0.5, C = 0.0129, ε_0 = 1 and m = 0.4. The quantity θ^{*} is related to a reference temperature and material melting point, which are 294.3 K and 1905 K, respectively. Additionally, the density, thermal conductivity, specific heat and coefficient of thermal expansion were given by 4424 kg/m^3, 6.566 W/m.K, 586.4 J/kg.K and 0.27e-4, respectively. Figure 2b shows the constitutive relationship for the titanium alloy.

Two sets of FEA were performed, described in Table 1. The first set, consisting of 10 calculations,

examined convergence of the computed peak equivalent plastic strain in the model. Three levels of mesh refinement (coarse (C), intermediate (I) and fine (F)) were considered for α = 1°, 3° and 6°. The corresponding element edge lengths were 100 μm, 50 μm and 25 μm.

Table 1. Fully coupled thermomechanical FE calculations performed to examine convergence of β (set 1) and enable comparison of computed and numerical load-displacement curves (set 2)

set	α (°)	mesh refinement	velocity (m/s)	simulation time (μs)
1	0	coarse	10[a]	182
	1	coarse	10[a]	130
	1	intermediate	10[a]	130
	1	fine	10[a]	130
	3	coarse	10[a]	75
	3	intermediate	10[a]	75
	3	fine	10[a]	75
	6	coarse	10[a]	35
	6	intermediate	10[a]	35
	6	fine	10[a]	35
2	0	intermediate	18[b]	until failure based on theory
	3	intermediate	18[b]	until failure based on theory
	6	intermediate	18[b]	until failure based on theory
			a – no rise time b – 20 μs rise time	

With α = 0°, only one mesh (intermediate refinement) was considered since convergent solutions with the stronger non-linearities (α = 1°, 3°) can be reasonably considered to imply same for the weakest non-linearity (α = 0°). The intermediate tilt value α = 1° was not tested in the laboratory but was analyzed for additional clarification of the evolution of the strain field non-linearity as a function of tilt. In this set of 10 calculations, a constant velocity of 10 m/s was applied to the top surface of the model and the simulations were run for 182 μs, 130 μs, 75 μs and 35 μs for α = 0°,1°, 3° and 6°, respectively. The simulation times were determined iteratively so as to achieve a maximum local equivalent strain of ~21–22 % in the model. This value of strain was chosen for its proximity to the strain corresponding to the maximum stress in the material stress-strain curve (25%), after which localization proceeds according to the present theory. In other words, convergence of the solution was examined not only in the relatively linear range of the material response but also in the critical non-linear region, which is more difficult to ensure.

Following the examination of convergence, a second set of calculations (see Table 1) was performed for purposes of direct comparison with the experimental load-displacement results. These calculations were performed for α = 0°, 3° and 6° and the intermediate level of mesh refinement only; boundary conditions were modeled after conditions imposed during the laboratory experiments (see Table 1), which included a 20 μs rise time and contact loading by the Hopkinson bars. A friction coefficient of 0.1 was used in these calculations. The simulation times correspond to the observed durations for the onset of stress collapse with the 0°, 3° and 6° tilted specimens.

4. Results

Split Hopkinson Compression Bar Experiments. The measured velocity (loading) spectra applied to the tilted cuboidal specimens with α = 0°, 3° and 6° are shown in Figure 3a. Following a brief rise-time, the average velocity imparted to the compression specimens is ~18 m/s. Figure 3b shows the measured engineering stress-strain curves obtained from the experiments; data for a standard cylindrical specimen with 0° tilt is also shown for reference.

Convergence of Maximum Local Equivalent Plastic Strain. Figure 4 and Table 2 summarize computed values of the maximum equivalent plastic strain, ε_{max}, obtained with the 3 levels of mesh refinement for the four values of tilt considered. The maximum value of the equivalent plastic strain occurs at the obtuse-angled corners of the specimens, as seen in Figure 4. Table 2 lists the values of maximum equivalent plastic strain from the 9 calculations prior to localization.

For α = 1°and 3°, the difference in solutions obtained with the coarse, intermediate and fine meshes is less than 5 %. However, for α = 6°, the maximum equivalent plastic strain does not converge. The amplification of the nominal strain is greatest for α = 6° is responsible for the observed lack of convergence with this level of perturbation. The meshes developed for α = 1° and 3° provide solutions that differ by less than 5% but the meshes developed for α = 6° differ by about 20 %.

Table 2. Maximum local equivalent strain, ε_{max}, values obtained with the 3 levels of mesh refinement for α = 0°, 1°, 3° and 6°. Nominal strain, ε_N, values were determined iteratively so as to generate $\varepsilon_{max} \approx$ 21–22%.

	coarse mesh	intermediate mesh	fine mesh
α = 0° (ε_N = 18.2%)	—	22.49%	—
α = 1° (ε_N = 13%)	21.48%	22.56%	22.8%
α = 3° (ε_N = 7.5%)	21.42%	22.22%	22.57%
α = 6° (ε_N = 3.5%)	19.19%	23.71%	28.12%

Convergence of Local Strain Rate Perturbation (β). The present theory can predict the timing of stress collapse based on the local strain rate perturbation, β, defined as $\beta^i = \frac{\dot{\varepsilon}^i - \dot{\varepsilon}^{avg}}{\dot{\varepsilon}^{avg}} \geq 0$ (2). Convergence of this quantity is shown in Table 3.

Table 3. Maximum strain rate perturbation, β, values obtained with the 3 levels of mesh refinement for α = 0°, 1°, 3° and 6°. The quantity β_ε, based on the equivalent strain instead of the equivalent strain rate, is also shown.

	β(x 10^2)			β_ε(x 10^2)		
α (°)	C	I	F	C	I	F
0	—	0.019	—	—	0.02	—
1	5.78	5.96	6.02	4.82	4.89	4.95
3	14.2	15.5	15.6	12.6	13.2	15.6
6	23.1	24.8	26.7	22.1	22.9	23.6

Failure Predictions. Using the computed values of β shown in Table 3, corresponding theoretical predictions of collapse strains can be obtained from Eq. (1) and the material properties described in section 3. These are shown in Table 4.

Table 4. Predicted values of strain corresponding to stress collapse, ε_f, in the tilted cuboidal specimens with α = 0°, 1°, 3° and 6°

α (°)	β	scale factor	ε_f
0	0.019e-2	0.075	0.55
3	15.6e-2	0.075	0.39
6	26.7e-2	0.075	0.35

These values of failure strain can be supplied to finite element models of the tilted cuboidal specimens loaded by the Hopkinson bars to obtain force-time plots that can be compared directly with the experimental results, shown in Figure 5.

5. Discussion and Conclusions

Comparison of the experimental and computed force-time plots indicates broad agreements as well as noticeable differences. Prior to stress collapse, the computed and measured initial non-linear rise in force and post-yield hardening (slope) are in good agreement with each other. However, the test results indicate a systematic decrease in the initial yield point with increasing tilt, which is not reflected in the calculations. The absence of additional information pertaining to the repeatability of the tests and variation in the material properties precludes any definitive conclusions as to the origins or statistical significance of this feature.

The sharp decline in force in Figure 5 corresponds to complete loss of load-carrying capacity in the specimen. Comparison with the predicted timings of stress collapse indicates that the *onset* of shear localization preceded total failure, which is reasonable. While this result supports the validity of the present model, additional factors remain to be explored in order to fully quantify its accuracy. Some of these relate to the variation of β, which is a function of local strain rate and strain – these in turn are dependent on the initial perturbation itself. In the present work, β has been evaluated at the nominal (applied) strain rate, which can be different from the local value. Also, the evolution or convergence of β as the deformation approaches the strain corresponding to the peak in the adiabatic stress-strain curve has yet to be examined.

The present results also show that convergence of the strain field may not be possible for all perturbations (6° tilt, for example). This aspect is not a limitation of the present model itself but limits its applicability to situations for which a reliable numerical solution can be obtained. The finding that the convergence of the local strain rate perturbation (β) is faster than that of the strain warrants additional study. It is significant from the standpoint of mesh refinement necessary when implementing the present model – it appears possible that a mesh for obtaining a converged strain rate perturbation may be *coarser* than one that provides the parent strain field.

Acknowledgments

The computational portion of this work was supported by Programming Environment & Training program within the US Department of Defense High Performance Computing Modernization Program. The authors are grateful to Dr. T. Weerasooriya for guidance with the experiments.

References

1. Wright, T.W., *The physics and mathematics of adiabatic shear bands*. Cambridge University Press, ISBN 0-521-63195-5/0521631955), United Kingdom, 2002.

2. Schoenfeld, S. and T.W. Wright, "A failure criterion based on material instability." *International Journal of Solids and Structures*, vol. 40, No. 12, 2003, pp. 3021–3037.

3. Meyer, L.W., E. Staskewitsch, and A. Burblies, "Adiabatic shear failure under biaxial dynamic compression/shear loading." *Mechanics of Materials*, 17, 1994, pp. 203–214.

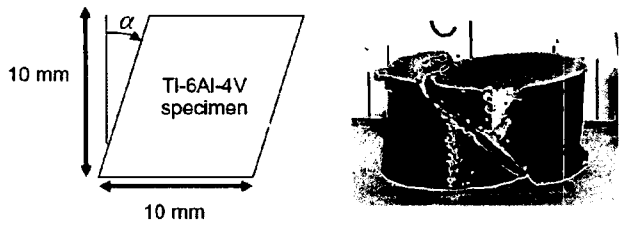

Figure 1. Schematic of Ti-6Al-4V cuboidal specimens used in split Hopkinson bar experiments with α = 0°, 3° or 6°. The photograph shows a typical specimen after failure through shear localization.

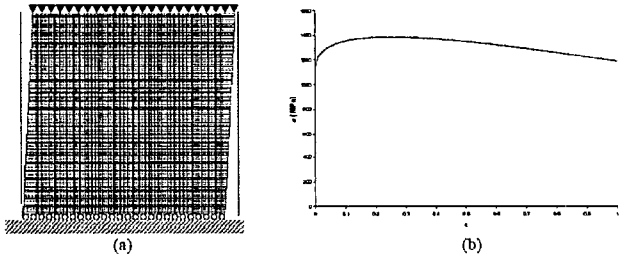

Figure 2. a) Finite element model of a 3°-tilted cuboid at the coarse level of refinement. Boundary conditions imposed are also indicated. b) Adiabatic stress-strain curve for the Ti-6Al-4V alloy (at a strain rate of 1000/s) used in the computations.

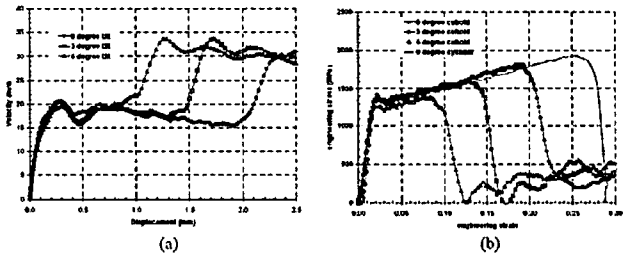

Figure 3. a) Velocity-displacement obtained from the tests with 0°, 3° and 6° tilted cuboidal specimens; b) Measured load-displacement curves obtained from the tests with 0°, 3° and 6° tilted cuboidal specimens

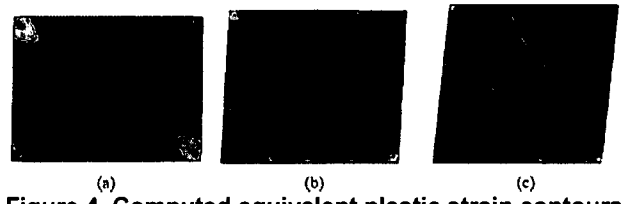

Figure 4. Computed equivalent plastic strain contours prior to localization (21–22% local strain) for: a) 1° tilted specimen (ε_N = 13 %), b) 3° tilted specimen (ε_N = 7.5 %), and c) 6° tilted specimen (ε_N = 3.5 %)

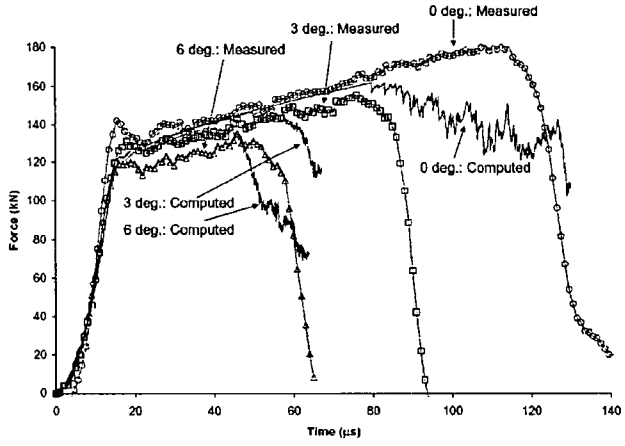

Figure 5. Comparison of measured and computed force-time curves for the 0°, 3° and 6° tilted cuboidal specimens